

# Effect of praseodymium oxide and cerium–praseodymium mixed oxide in the Pt electrocatalyst performance for the oxygen reduction reaction in PAFCs

Q. He · S. Mukerjee · S. Parres-Eslapez ·  
A. Bueno-López

Received: 5 February 2011 / Accepted: 7 April 2011 / Published online: 22 April 2011  
© Springer Science+Business Media B.V. 2011

**Abstract** The effect of praseodymium oxide and cerium–praseodymium mixed oxide in the Pt electrocatalyst performance for oxygen reduction reaction (ORR) in Phosphoric Acid Fuel Cells (PAFCs) has been studied. Three electrocatalysts (Pt/C, PtPrO<sub>x</sub>/C and PtCe<sub>0.9</sub>Pr<sub>0.1</sub>O<sub>y</sub>/C, where  $x$  and  $y$  are  $\leq 2$ ) have been prepared and tested by cyclic voltammetry (CV) and long term chronoamperometry (CA) experiments. The fresh and tested electrocatalysts have been characterized by X-ray diffraction (XRD) and Transmission Electron Microscopy–Energy Dispersion Spectroscopy (TEM–EDS). The Pr and Ce–Pr oxides improved Pt dispersion in the fresh electrocatalysts with regard to the Pt-only catalyst, and the PtPrO<sub>x</sub>/C and PtCe<sub>0.9</sub>Pr<sub>0.1</sub>O<sub>y</sub>/C electrocatalysts presented a slightly improved catalytic activity towards ORR in comparison to the reference Pt/C electrocatalyst. The activity decay during the long term CA tests was slower for PtPrO<sub>x</sub>/C and PtCe<sub>0.9</sub>Pr<sub>0.1</sub>O<sub>y</sub>/C than for Pt/C. Although the Pr and Ce–Pr oxides were dissolved during the CA measurements, the Pt sintering was prevented.

**Keywords** PAFCs · ORR · Platinum · Metal oxides · Praseodymium · Cerium oxide · Ceria

## 1 Introduction

Due to their high reliability, Phosphoric Acid Fuel Cells (PAFCs) represent, for some applications, the answer to electricity quality and availability needs. These power plants require less maintenance than competing conventional power generators of similar size, like gas engines or gas turbines. In addition, the state-of-the-art Pt based catalysts used in PAFCs are tolerant to higher CO concentration at a typical running temperature of 200 °C. For all these reasons, more than 500 PAFC power plants have been installed and tested around the world since the 1970s [1].

In a PAFC, hydrogen or a hydrogen rich gas mixture is provided to the anode, where it is oxidized to form protons and electrons. The protons migrate from the anode to the cathode through the electrolyte (H<sub>3</sub>PO<sub>4</sub>, a proton conductor) and the electrons migrate through an external circuit. Air is provided at the cathode, and the oxygen reduction reaction (ORR) takes place by reaction of oxygen with the protons coming from the electrolyte and the electrons coming from the external circuit. In order to find a compromise between electrolyte conductivity which increases with temperature and cell life which decreases with temperature, the operating temperature of PAFCs is typically fixed at 150–200 °C.

Since the 1960s, when the earliest PAFCs were developed, high surface area Pt is the most important noble metal electrocatalyst used on both the anode and the cathode. However, one of the main drawbacks of high surface area Pt for the PAFCs application is the

Q. He · S. Mukerjee  
Department of Chemistry & Chemical Biology, Northeastern University, 360 Huntington Ave, Boston, MA 02115, USA

S. Parres-Eslapez · A. Bueno-López (✉)  
Department of Inorganic Chemistry, University of Alicante, Ap. 99, 03080 Alicante, Spain  
e-mail: agus@ua.es

*Present Address:*

Q. He  
Lawrence Berkeley National Lab, Environmental Energy Technologies Division, 1 Cyclotron Road Mail Stop 70-108B, Berkeley, CA 94720, USA

agglomeration of Pt nanoparticles on the surface of the carbon support at high temperature which reduces the active surface area. Alloying of Pt with other metals is one of the strategies developed to improve the stability of Pt [2], and several alloys have been investigated to improve the Pt performance under PAFCs operating conditions, such as Pt–V [3, 4], Pt–Cr [5, 6], Pt–Co [7] or Pt–Cr–Co ternary alloys [8–10], among others.

Recently [11],  $\text{PtMO}_2/\text{C}$  ( $\text{M} = \text{Ce}, \text{Zr}, \text{Ce}_{0.9}\text{Zr}_{0.1}$ ) electrocatalysts were prepared and tested as cathode materials for ORR under PAFCs operating conditions. Although, the  $\text{MO}_2$ -promoted Pt electrocatalysts offered marginally better kinetic performances in comparison to  $\text{Pt}/\text{C}$ , the stability of Pt was improved significantly in the presence of  $\text{MO}_2$ . The most stable electrocatalyst, among those tested, was the electrocatalyst loaded with the mixed oxide  $\text{Ce}_{0.9}\text{Zr}_{0.1}\text{O}_2$ . The fairly close Tafel slope values for ORR with  $\text{PtMO}_2/\text{C}$  catalysts in the high overpotential region and the low overpotential region indicated that metal oxides preserved Pt active sites and prevented the Pt surface from oxidation. It was also concluded that the incorporation of metal oxides hindered sintering of Pt nanoparticles significantly. Formation of a core–shell structure and an unusual passivation phenomenon pertinent to mixed oxides were proposed to explain the excellent stability of  $\text{PtCe}_{0.9}\text{Zr}_{0.1}\text{O}_2/\text{C}$  in an environment mimicking real operation conditions in PAFCs.

As another rare earth element, praseodymium presents some properties that mimic those of cerium. Both cerium and praseodymium are able to form cations with 3+ and 4+ oxidation states and have very similar cation sizes (0.97 and 0.96 Å for  $\text{Ce}^{4+}$  and  $\text{Pr}^{4+}$ , respectively, and 1.14 and 1.13 Å for  $\text{Ce}^{3+}$  and  $\text{Pr}^{3+}$ , respectively). Consequently, the high compatibility between Ce and Pr cations allows formation of a solid solution of type  $\text{Ce}_x\text{Pr}_{1-x}\text{O}_y$  with very interesting catalytic properties. For instance, it has been demonstrated that  $\text{Ce}_x\text{Pr}_{1-x}\text{O}_y$  catalysts are very active in diesel soot combustion [12–14], and also that Ce–Pr mixed oxides are active promoters of the catalytic activity of Rhodium in  $\text{N}_2\text{O}$  decomposition [15].

The aim of the current study is to extend the conclusions previously obtained with  $\text{PtMO}_2/\text{C}$  ( $\text{M} = \text{Ce}, \text{Zr}, \text{Ce}_{0.9}\text{Zr}_{0.1}$ ) electrocatalysts to Pt electrocatalysts loaded with a praseodymium oxide or with a cerium–praseodymium mixed oxide.

## 2 Experimental

### 2.1 Preparation of the electrocatalyst active phases

Three electrocatalysts were prepared in this study, which are referred to as  $\text{Pt}/\text{C}$ ,  $\text{PtPrO}_x/\text{C}$  and  $\text{PtCe}_{0.9}\text{Pr}_{0.1}\text{O}_y/\text{C}$ ,

respectively. The materials used to prepare the active phases of these electrocatalysts were powder carbon black (C) from Cabot (Vulcan XC72),  $\text{Pt}(\text{NH}_3)_4(\text{NO}_3)_2$  (Sigma-Aldrich, 99.995%),  $\text{Ce}(\text{NO}_3)_3 \cdot 6\text{H}_2\text{O}$  (Sigma-Aldrich, 99.99%) and  $\text{Pr}(\text{NO}_3)_3 \cdot 6\text{H}_2\text{O}$  (Sigma-Aldrich, 99.9%).

The preparation procedure of the powder active phases is similar to that recently described for ceria and ceria–zirconia-containing Pt electrocatalysts [11]. Briefly, the carbon black was dispersed in a water–ethanol solution of the praseodymium and/or cerium + praseodymium precursors. The proper concentration of these solutions was chosen to achieve 10 wt% of Pr and 10 wt% of Ce + Pr in the electrocatalysts  $\text{PtPrO}_x/\text{C}$  and  $\text{PtCe}_{0.9}\text{Pr}_{0.1}\text{O}_y/\text{C}$ , respectively. Ammonia was dropped until  $\text{pH} = 9$  to promote the precipitation (or co-precipitation) of the metal hydroxides, and the samples were dried at 110 °C and heat-treated at 500 °C for 2 h under  $\text{N}_2$  flow. Pt was impregnated on C, Pr/C and CePr/C afterwards with a target loading of 10 wt% in all samples. Finally, the samples were dried at 110 °C and heat-treated at 500 °C for 2 h under  $\text{N}_2$  flow.

### 2.2 Electrode preparation and electrochemical measurements

A sleeveless rotating disk electrode setup, from Pine Instruments, connected to an Autolab potentiostat (Ecochemie Inc. Model-PGSTAT 30) was employed to study the ORR kinetics of Pt electrocatalysts in concentrated phosphoric acid at 110 °C. A cylindrical gold electrode without an isolating mantel to establish hydrodynamic flow was used. The electrode was introduced into the glass cell until it just touched the electrolyte surface. A photograph of the setup used was shown in a previous publication [11] and a scheme is included in Fig. 1. The electrolyte was  $\text{H}_3\text{PO}_4$  (Sigma-Aldrich), purified using the standard procedure described in the literature [16]. A dynamic hydrogen electrode (DHE) was used as the reference electrode. The same method described in a previous paper [17] was followed to prepare catalyst inks and electrodes modified with various catalysts. A gold electrode with a diameter of 5 mm was used as the substrate for the catalysts. The depth of gold cylinder in the electrolyte solution was carefully controlled by a dial gauge and set at 0.3 mm for all experiments. A subsequent total active area of 0.243 cm<sup>2</sup> was used to calculate current density for all experiments. The catalyst film was prepared by dispersing 8 µL of the catalyst ink on the gold substrate. The catalysts had a Pt loading of about 8.3 µg (Pt) cm<sup>-2</sup> that was bound with Nafion® (DuPont, Wilmington DE, 8 µL of 0.12 wt% Nation® solution diluted with isopropanol) onto the end of the gold electrode. The Nafion layer is about 0.06 µm, resulting in negligible diffusion limitation to ORR

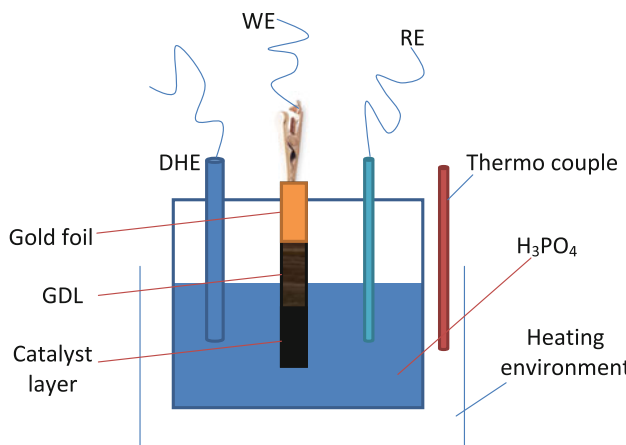


**Fig. 1** Scheme of the setup used for the electrochemical measurements. The catalyst layer is under the level of electrolyte ( $\text{H}_3\text{PO}_4$ ). The gold foil was used to prevent any contact of the alligator clip with the electrolyte

measurement [18]. The kinetic currents were derived from the disk currents (cathodic scans) at a rotation speed of 1600 rpm corrected by mass transport limitation. The potential was swept with a scan rate of  $20 \text{ mV s}^{-1}$ . Long term (24 h) chronoamperometry (CA) tests were also carried out. Catalyst inks, prepared as described in our previous paper [17], were painted onto gas diffusion layer (GDL, HT1400®, HT 1400, from E-TEK, New Jersey, U.S.A.) and dried at  $60^\circ\text{C}$  in vacuum for 2 h. One piece of GDL ( $1.9 \text{ cm} \times 1.3 \text{ cm}$ ) with Pt loading of  $0.3 \text{ mg cm}^{-2}$  was used as the working electrode. Long term CA tests were conducted on all catalysts in a three-electrode cell containing  $\text{O}_2$  saturated  $\text{H}_3\text{PO}_4$  solution at  $110^\circ\text{C}$  and  $0.88 \text{ V}$  (versus DHE). A platinum wire and a dynamic hydrogen electrode were used as the counter and reference electrodes. Cyclic voltammograms (CVs) and polarization curves for ORR were taken both before and after the long term CA tests on all samples.

### 2.3 Characterization of electrocatalysts by XRD and TEM

X-ray diffraction (XRD) studies of the electrocatalyst powders and the electrodes loaded with these active phases were performed in a Rigaku diffractometer using  $\text{Cu K}\alpha$  radiation ( $\lambda = 0.15418 \text{ nm}$ ). The diffraction studies and phase characterizations were performed before and after the long term CA tests.

A JEOL (JEM-2010) transmission electron microscope (TEM), equipped with an Energy Dispersive X-ray analyser (EDS by OXFORD, model INCA Energy TEM100), was used to obtain TEM images of the samples before and after the long term CA tests. To prepare the samples for TEM characterization, the electrodes were put in contact

with ethanol and ultrasonically dispersed suspensions of the active phases were obtained. A few droplets of these suspensions were placed on a copper grid with lacey carbon film and dried at ambient conditions. In this case, the electrodes were also characterized before and after the long term CA tests.

The size distribution of Pt particles was estimated from TEM images. Typically, three representative pictures were selected for each electrocatalyst, taken at magnification factors of  $\times 25,000$ ,  $\times 100,000$  and  $\times 300,000$ . The software *AnalySIS*, by Olympus Soft Imaging Solutions, was used to measure the size of the Pt particles. The number of Pt particles measured varied with the samples, and it ranged from 300 to 1000 particles to ensure statistical significance.

## 3 Results and discussion

### 3.1 Kinetics performance for ORR

Figure 2 shows the CVs of Pt/C,  $\text{PtPrO}_x/\text{C}$  and  $\text{PtCe}_{0.9}\text{Pr}_{0.1}\text{O}_y/\text{C}$  catalysts in purified 85%  $\text{H}_3\text{PO}_4$  at room temperature. The background signal from the gold electrode is negligible. The upper limit of the potential sweep range for the catalyst of  $\text{PtPrO}_x/\text{C}$  was lowered slightly to  $1.0 \text{ V}$  (versus DHE) to avoid possible catalyst degradation associated with severe dissolution of Ce at high potentials [11, 19]. The features of typical crystal planes of Pt in the H up region were suppressed due to adsorption of phosphate anions on highly dispersed Pt nanoparticle surfaces [20, 21]. The electrochemical surface area (ECA) of Pt was calculated from both integrations of the hydrogen adsorption and desorption peaks assuming a correlation value of  $210 \mu\text{C cm}^{-2}$  [22]. Average results of two independent measurements are tabulated in Table 1. Little variation of the ECA may reflect the similarity of particle size and dispersion of the as-synthesized catalysts.

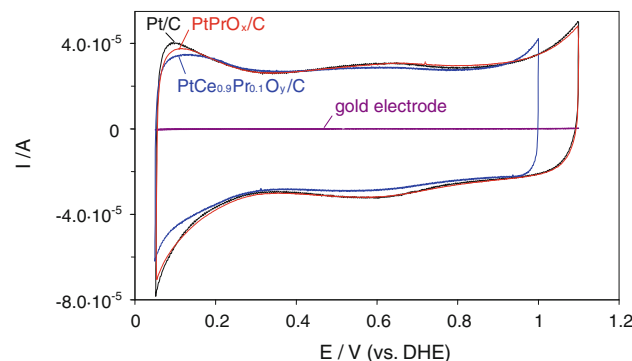


**Fig. 2** Cyclic voltammograms for Pt/C,  $\text{PtPrO}_x/\text{C}$ ,  $\text{PtCe}_{0.9}\text{Pr}_{0.1}\text{O}_y/\text{C}$  in 85%  $\text{H}_3\text{PO}_4$  purged with Ar at room temperature, scan rate:  $50 \text{ m s}^{-1}$

**Table 1** Electrochemical characterization of the electrocatalysts by CV and RDE

|                                     | ECA ( $\text{m}^2 \text{ g}^{-1}$ ) | $n$  | $E_{1/2}$ (V) | Slope of Tafel plots (mV dec $^{-1}$ ) | Kinetics current density at 0.875 V (mA cm $^{-2}$ ) |
|-------------------------------------|-------------------------------------|------|---------------|--|--|
| Pt/C                                | 27.3                                | 3.96 | 0.798         | 64.2/125.1                             | 0.104  |
| PtPrO $_x$ /C                       | 26.3                                | 3.83 | 0.780         | 128.5/129.2                            | 0.130  |
| PtCe $_{0.9}$ Pr $_{0.1}$ O $_y$ /C | 26.1                                | 4.0  | 0.799         | 113.2/126.3                            | 0.116  |

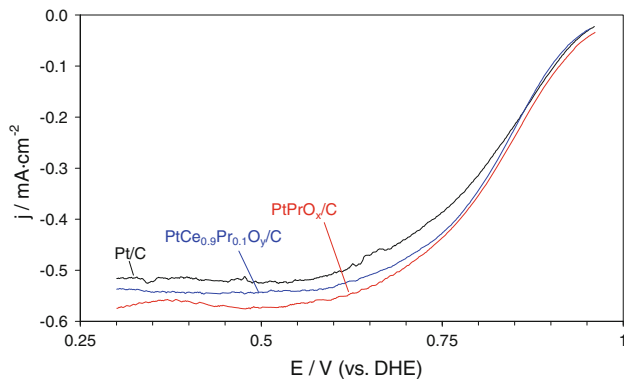
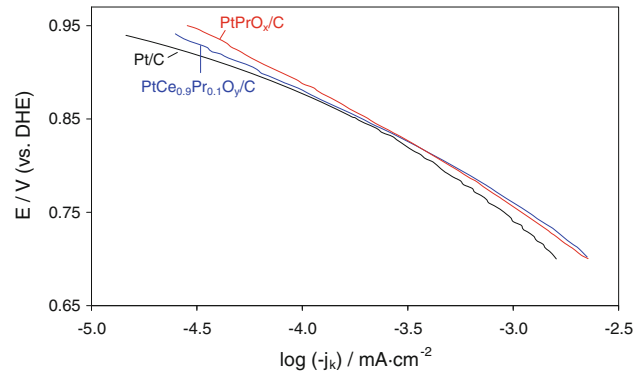
**Fig. 3** Rotating disk data (cathodic scans) for all Pt catalysts in purified 85%  $\text{H}_3\text{PO}_4$  saturated with  $\text{O}_2$  at 110 °C, scan rate: 20 mV s $^{-1}$ , rotation rate: 1600 rpm, with 15  $\mu\text{g cm}^{-2}$  of Pt loading on the electrode

Figure 3 shows the disk electrode polarization curves for ORR on Pt/C, PtPrO $_x$ /C and PtCe $_{0.9}$ Pr $_{0.1}$ O $_y$ /C catalysts at 1600 rpm at an elevated temperature (110 °C) in concentrated phosphoric acid (85%). Three well-defined regions can be identified, namely, a kinetics controlled region (>+0.9 V), a mixed diffusion-kinetic limitation region (+0.65 to +0.9 V) and a diffusion-controlled region (<+0.65 V). Derived from data in Fig. 3, the semi-log plots of the potential versus the kinetic current shown in Fig. 4 were made to achieve the Tafel slopes for ORR on as-synthesized catalyst materials. From Fig. 4 and Table 1, slight improvement in the catalytic activity of PtPrO $_x$ /C and PtCe $_{0.9}$ Pr $_{0.1}$ O $_y$ /C compared to Pt/C can be observed. These results are in agreement with those obtained previously with PtMO $_2$ /C (M = Ce, Zr or Ce $_{0.9}$ Zr $_{0.1}$ ) [11]. Moreover, it has been confirmed from our previous study that the O $_2$  diffusional effect on Tafel slopes related to the electrode thickness can be omitted under the overall ambit of catalyst loadings from 3.0 to 10.4  $\mu\text{g}$  (Pt) cm $^{-2}$  [11]. Therefore, the diffusion-free intrinsic catalytic activity for ORR can be evaluated here. [18, 23, 24]. Two typical Tafel slopes of  $-125.1$  and  $-64.2$  mV dec $^{-1}$  can be observed on the Tafel plot for Pt/C, which can be ascribed to a combination of both “energetic effects” (changing of adsorption isotherm for reaction intermediate from Temkin to Langmuir adsorption) [11, 25–27] and “blocking effects” (surface coverage of oxygen containing species controlling availability of O $_2$ ) [28].

**Fig. 4** Tafel plots obtained from disk current for Pt/C, PtPrO $_x$ /C, and PtCe $_{0.9}$ Pr $_{0.1}$ O $_y$ /C in 85%  $\text{H}_3\text{PO}_4$  saturated with  $\text{O}_2$  at 110 °C, rotation rate: 1600 rpm

adsorption) [11, 27]. Further, it is interesting to note that the deviation of Tafel slopes in the low current density region from that in high current density region on PtPrO $_x$ /C and PtCe $_{0.9}$ Pr $_{0.1}$ O $_y$ /C is very little. It clearly indicates that the PtOH film formation leading to a lower Tafel slope was greatly inhibited due to a sacrificial Ce or Pr oxidized effect [11, 28]. In other words, the Pt active sites can be preserved with oxidation of Ce or Pr at relatively low potential.

### 3.2 Durability performance for ORR

Figure 5 shows the performance of Pt/C, PtPrO $_x$ /C and PtCe $_{0.9}$ Pr $_{0.1}$ O $_y$ /C catalysts during the long term CA tests in hot H $_3$ PO $_4$  (110 °C) at 0.88 V (versus DHE). Quasi-exponential current decays can be observed, which may be attributed to the diffusion limitation of O $_2$  in phosphoric acid as well as degradation and dissolution of some catalyst components [11, 29, 30]. A driving force for dissolution of Pr or Ce oxides may be the concentration difference of the metal cations between the electrode surface and the bulk solution. Nevertheless, PtPrO $_x$ /C and PtCe $_{0.9}$ Pr $_{0.1}$ O $_y$ /C still gave slower decay of current and higher values of total charge transferred as shown in Table 2. Furthermore, the rates of reduction of ECA and peak power density after long term CA tests on Pt/C, PtPrO $_x$ /C and PtCe $_{0.9}$ Pr $_{0.1}$ O $_y$ /C catalysts can be seen in Figs. 6, 7 and Table 2. The more durable performance for ORR found on the PtPrO $_x$ /C and PtCe $_{0.9}$ Pr $_{0.1}$ O $_y$ /C electrocatalysts over Pt/C is quite unusual,

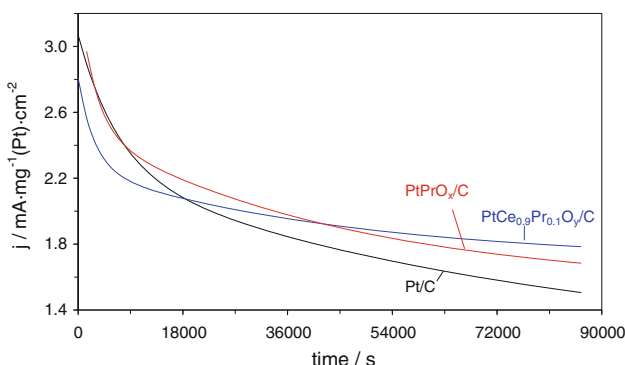


**Fig. 5** Chronoamperometric profiles for Pt/C, PtPrO<sub>x</sub>/C and PtCe<sub>0.9</sub>Pr<sub>0.1</sub>O<sub>y</sub>/C in 85% H<sub>3</sub>PO<sub>4</sub> saturated with O<sub>2</sub> at 110 °C, working area of electrode: 1.1 cm<sup>2</sup>

since the used oxides (PrO<sub>x</sub> and Ce<sub>0.9</sub>Pr<sub>0.1</sub>O<sub>y</sub>) are less stable than Pt especially at high potentials close to 1 V [11, 19] and therefore more subject to corrosion than Pt in hot phosphoric acid. From the CA curves shown in Fig. 5, during the first three hours, PtPrO<sub>x</sub>/C showed almost identical performance with Pt/C. The current density on the Pt mixed metal oxides sample (PtCe<sub>0.9</sub>Pr<sub>0.1</sub>O<sub>y</sub>/C) decreased fairly rapidly as a function of time. It indicates that the surface oxide layers (PrO<sub>x</sub> and Ce<sub>0.9</sub>Pr<sub>0.1</sub>O<sub>y</sub>) had been completely dissolved within this time domain. Meanwhile, an ideal structure of dealloyed pure Pt shell with Pt metal oxides alloy core may be formed. The bond energy of these intermetallic compounds is so high ( $-250 \text{ kJ mol}^{-1}$ ) that further dissolution of Pt can be prevented [31, 32]. This plausible mechanism is nicely corresponding to slower decay of current density on PtPrO<sub>x</sub>/C and PtCe<sub>0.9</sub>Pr<sub>0.1</sub>O<sub>y</sub>/C than Pt/C in the second time domain (3–24 h). In addition, as it is demonstrated in the next section, Pt dispersion remained high on the PtPrO<sub>x</sub>/C and PtCe<sub>0.9</sub>Pr<sub>0.1</sub>O<sub>y</sub>/C electrocatalysts, while Pt on Pt/C sintered significantly under reaction conditions. It may also render less long term loss in catalytic activity on the Pt metal oxide catalysts than Pt/C.

### 3.3 XRD and TEM characterization

The active phases of the powder samples and the electrodes before and after the long term CA tests were characterized by XRD (Fig. 8). All the fresh and used electrodes present

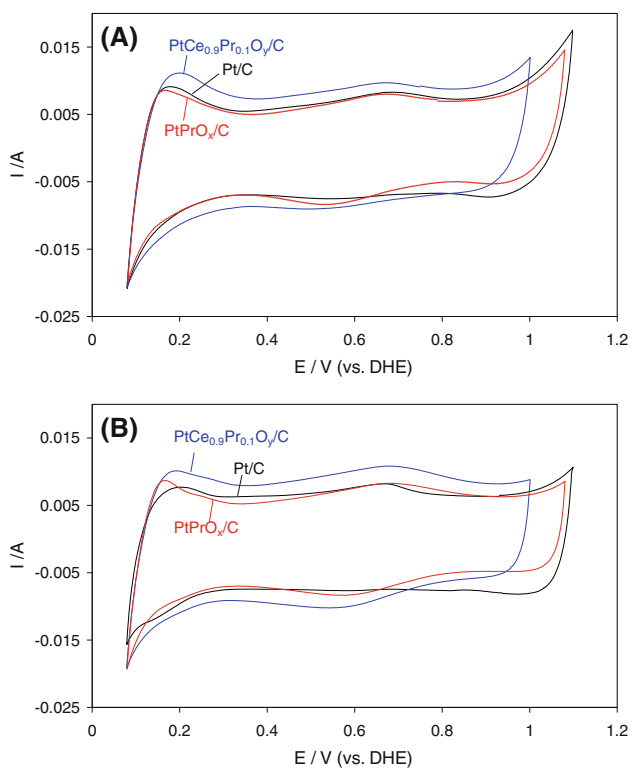


**Fig. 6** Cyclic voltammograms for Pt/C, PtPrO<sub>x</sub>/C and PtCe<sub>0.9</sub>Pr<sub>0.1</sub>O<sub>y</sub>/C on GDL in 85% H<sub>3</sub>PO<sub>4</sub> purged with Ar at 110 °C **a** before and **b** after 24 h CA test, scan rate: 50 mV s<sup>-1</sup>

peaks of both graphite (plane (002) at 26.0°) and Pt (planes (111), (200), (220) and (311) at 39.9°, 46.4°, 67.7° and 81.5°, respectively) [33]. A narrow peak at 18.2° and another graphite peak at 43.6° due to GDL support can also be seen.

X-ray diffraction peaks due to metal oxides were also observed in some diffractograms. The XRD patterns of Pt/C and PtPrO<sub>x</sub>/C (Fig. 8b) show several diffraction peaks that can be attributed to a mixture of praseodymium oxides composed of Pr<sub>2</sub>O<sub>3</sub>, PrO<sub>2</sub> and a range of intermediate phases including Pr<sub>2</sub>O<sub>3</sub>, PrO<sub>1.670</sub>, PrO<sub>1.714</sub>, PrO<sub>1.780</sub>, PrO<sub>1.800</sub>, PrO<sub>1.810</sub>, and PrO<sub>1.833</sub> [34–36]. The powder Ce<sub>0.9</sub>Pr<sub>0.1</sub>O<sub>y</sub>/C and PtCe<sub>0.9</sub>Pr<sub>0.1</sub>O<sub>y</sub>/C samples (Fig. 8c) show typical reflections of the fluorite structure of ceria at 28.7°, 33.4°, 47.8° and 56.8° (planes (111), (200), (220) and (311), respectively) [37]. The absence of praseodymium oxide peaks in CePr/C

**Table 2** 24 h CA test in O<sub>2</sub> saturated hot H<sub>3</sub>PO<sub>4</sub> (110 °C) at 0.88 V (versus DHE)

|   | $Q (\text{C mg}^{-1} (\text{Pt}) \text{cm}^{-2})$<br>$t < 5 \text{ h}$ | $Q (\text{C mg}^{-1} (\text{Pt}) \text{cm}^{-2})$<br>$5 \text{ h} < t < 11 \text{ h}$ | $Q (\text{C mg}^{-1} (\text{Pt}) \text{cm}^{-2})$<br>$11 \text{ h} < t < 24 \text{ h}$ | $Q (\text{C mg}^{-1} (\text{Pt}) \text{cm}^{-2})$<br>$24 \text{ h}$ | ECA off % | Power density<br>off % |
|---|--|---|--|---|-----------|------------------------|
| Pt/C  | 41.4   | 36.4  | 74.4   | 152.2   | 22.2      | 13.4                   |
| PtPrO <sub>x</sub> /C                                   | 42.1   | 38.9  | 81.2   | 162.2   | 4.1       | 10.4                   |
| PtCe <sub>0.9</sub> Pr <sub>0.1</sub> O <sub>y</sub> /C | 38.7   | 37.9  | 83.7   | 160.3   | 7.7       | 7.0                    |

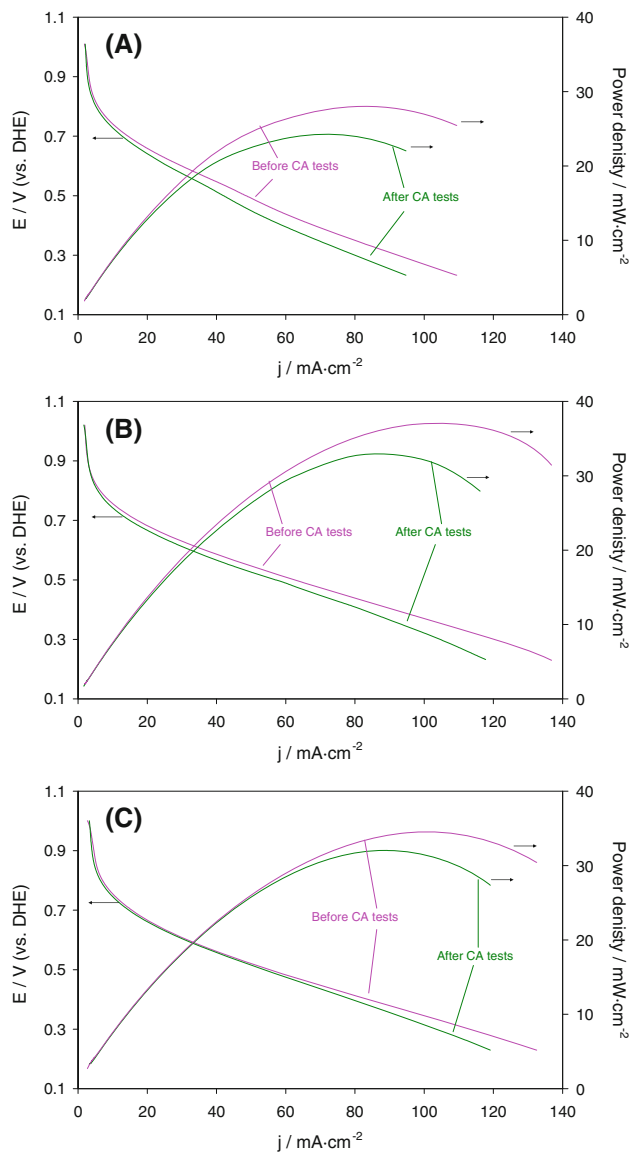


**Fig. 7** ORR polarization curves and power density curves on GDL before and after 24 h Chronoamperometry test in 85%  $H_3PO_4$ , at 110 °C. **a** Pt/C, **b** PtPrO<sub>x</sub>/C and **c** PtCe<sub>0.9</sub>Pr<sub>0.1</sub>O<sub>y</sub>/C

and PtCe<sub>0.9</sub>Pr<sub>0.1</sub>O<sub>y</sub>/C (Fig. 8c) is expected, since it is very efficient to dope cerium oxide with praseodymium cations to form Ce–Pr mixed oxides [12, 15].

The metal oxide diffraction peaks were also observed in the diffractograms of the fresh electrodes but not in the electrodes obtained after long term CA tests; thus confirming the dissolution of praseodymium oxides and Ce–Pr mixed oxides under the reaction conditions. The dissolution of MO<sub>2</sub> oxides was also observed previously in PtMO<sub>2</sub>/C electrodes with M = Ce, Zr and Ce<sub>0.9</sub>Zr<sub>0.1</sub> [11].

The removal of the praseodymium oxides and the Ce–Pr mixed oxide during the long term CA tests is further established by TEM–EDS characterization (Fig. 9; Table 3). EDS measurements were recorded and the data

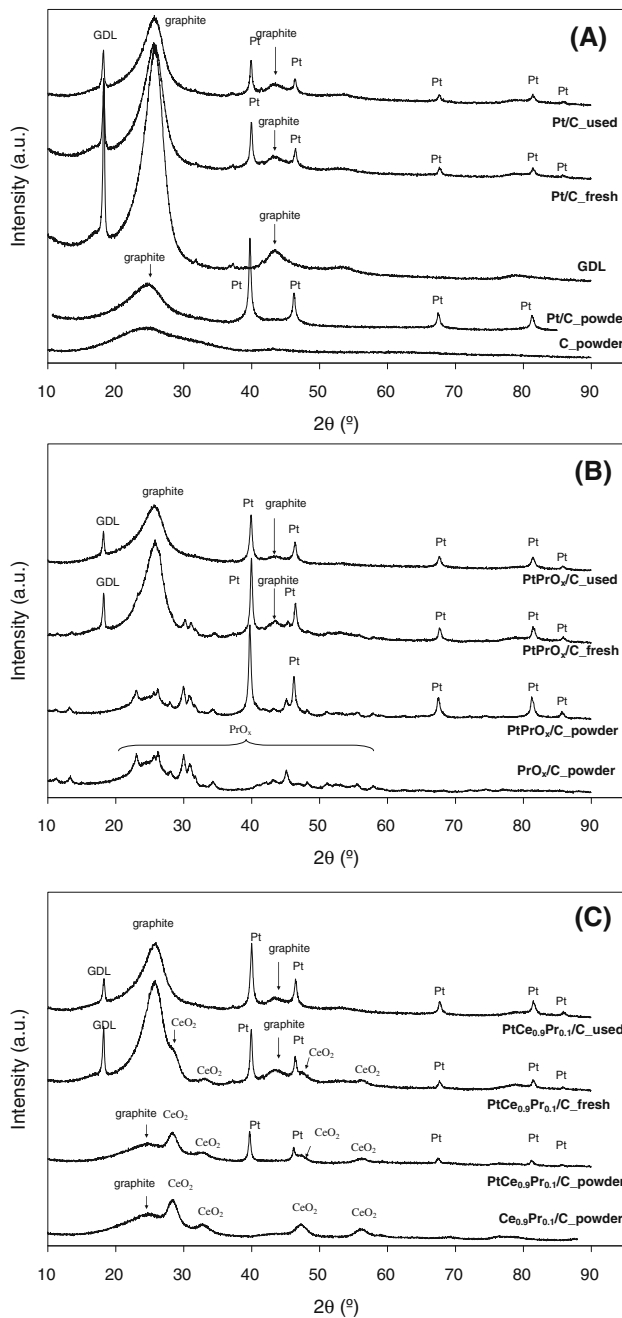


**Fig. 8** XRD characterization of the electrocatalysts with **a** none oxide, **b** PrO<sub>x</sub>, **c** Ce<sub>0.9</sub>Pr<sub>0.1</sub>O<sub>y</sub>

obtained for a single spot of each sample are compiled in Table 3. For a proper interpretation of the EDS data, it must be taken into account that the EDS analyses of Table 3 correspond to a particular area of each sample, and therefore, the values are not consistent with the nominal composition of the samples. For instance, the Pt percentage on the fresh and used Pt/C electrocatalyst (18.3 and 55.7 wt%) are well above the nominal percentage (10 wt%) because Pt-rich areas have been selected for the EDS analyses. On the other hand, the absence of Pr in the

**Fig. 9** TEM images of the electrocatalysts: **a** Pt/C\_fresh, **b** Pt/C\_used, **c** PtPrO<sub>x</sub>/C\_fresh, **d** PtPrO<sub>x</sub>/C\_used, **e** PtCe<sub>0.9</sub>Pr<sub>0.1</sub>O<sub>y</sub>/C\_fresh and **f** PtCe<sub>0.9</sub>Pr<sub>0.1</sub>O<sub>y</sub>/C\_used

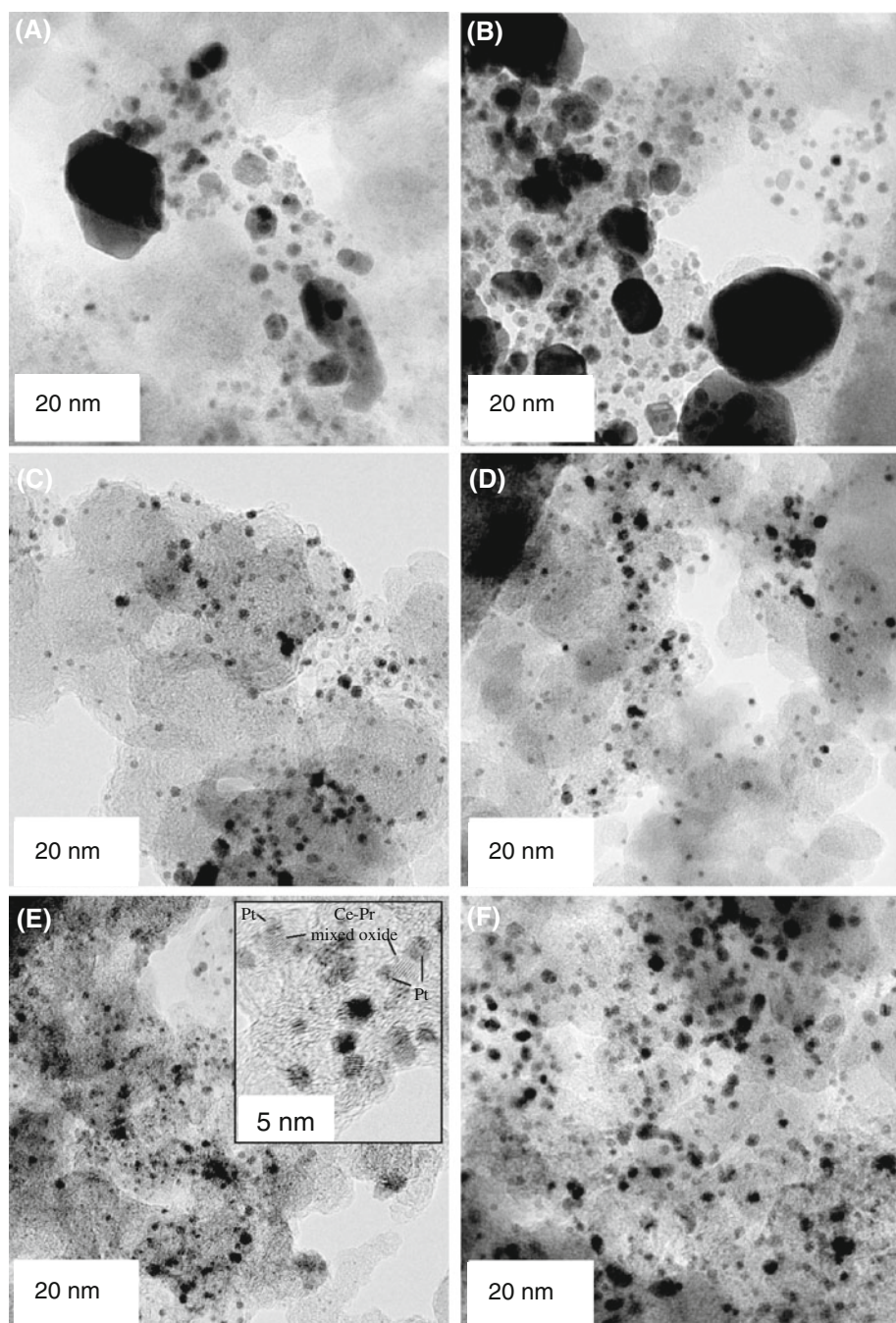


**Table 3** EDS analyses of fresh and used electrocatalysts

|   | Pt<br>(wt%) | Ce<br>(wt%) | Pr<br>(wt%) |
|---|-------------|-------------|-------------|
| Pt/C_fresh  | 18.3        | —           | —           |
| Pt/C_used   | 55.7        | —           | —           |
| PtPrO <sub>x</sub> /C_fresh                                   | 19.5        | —           | 4.4         |
| PtPrO <sub>x</sub> /C_used                                    | 14.4        | —           | —           |
| PtCe <sub>0.9</sub> Pr <sub>0.1</sub> O <sub>y</sub> /C_fresh | 3.0         | 1.1         | —           |
| PtCe <sub>0.9</sub> Pr <sub>0.1</sub> O <sub>y</sub> /C_used  | 5.4         | —           | —           |

“—” Not detected

EDS analysis of the fresh sample PtCe<sub>0.9</sub>Pr<sub>0.1</sub>O<sub>y</sub>/C can be attributed to the low concentration of this element. However, in spite of these limitations of the TEM-EDS technique, the EDS analyses confirm the presence of Pt, Ce, and/or Pr on the fresh electrodes, while the used electrodes only contained Pt, but neither Pr nor Ce, which confirms the dissolution of the metal oxides during the long term CA tests. The expected harmful effects of the dissolved Pr or Ce into the catalyst layer (change of pH, decrease of diffusion rate of O<sub>2</sub> in the electrolyte, etc.) for the potential use in PAFCs are still under investigation.

As can be deduced from the TEM images of the fresh samples, the distribution of Pt particles on the surface of the carbon support is very heterogeneous for the sample of Pt/C (Fig. 9a) and the Pr-containing oxides helped to improve Pt dispersion (Fig. 9c, e). For the fresh Pt/C sample (Fig. 9a), the distribution of particle sizes are in a range from around 1 nm to more than 40 nm. However, the particle size distributions for  $\text{PtPrO}_x/\text{C}$ \_fresh and  $\text{PtCe}_{0.9}\text{Pr}_{0.1}\text{O}_y/\text{C}$ \_fresh are much narrower. This is clearly demonstrated in Fig. 9c, e, where the former is in the range of size between 1 and 4 nm and the latter is in the range of size between 1 and 3 nm. The improved Pt dispersion is attributed to the Pt–metal oxide interactions, and as an example, the inset included in Fig. 9e ( $\text{PtCe}_{0.9}\text{Pr}_{0.1}\text{O}_y/\text{C}$ \_fresh) shows that Pt particles are attached to Ce–Pr oxide particles.

The TEM images taken after long term CA tests clearly demonstrate that Pt nanoparticles supported on the bare carbon sintered significantly during the CA tests. Most of the Pt nanoparticles are agglomerated and located in particular areas of the carbon support while there are large areas of the support without Pt as shown in Fig. 9b. On the other hand, the Pr-containing metal oxides hindered Pt sintering (Fig. 9d, f), in spite of the dissolution of the oxides under reaction conditions, and the high Pt dispersion remained even after the metal oxides leached to the reaction medium. It is interesting to find that the large Pt particles were poorly dispersed on the carbon support of the Pt/C electrocatalyst and sintered much more easily than the small Pt particles on  $\text{PtPrO}_x/\text{C}$  and  $\text{PtCe}_{0.9}\text{Pr}_{0.1}\text{O}_y/\text{C}$  with better dispersion of metal particles on the surface of the support. This finding seems to be contradictory to the well-known fact that sintering more readily occurs on smaller particles. An explanation is that a core (Pt oxide alloys)–shell (Pt) structure was formed after leaching of surface oxide layers. However, as-formed intermetallic compounds have very strong bond energy, which prevents the sintering of Pt nanoparticles.

The TEM-estimated Pt size distributions for the Pt/C,  $\text{PtPrO}_x/\text{C}$  and  $\text{PtCe}_{0.9}\text{Pr}_{0.1}\text{O}_y/\text{C}$  electrodes are included in Fig. 10. It is to be noted that the size distributions of the Pt nanoparticles on the fresh  $\text{PtPrO}_x/\text{C}$  and the fresh  $\text{PtCe}_{0.9}\text{Pr}_{0.1}\text{O}_y/\text{C}$  electrodes could not be determined because Pt nanoparticles could not be easily distinguished from those of the Pr and Ce–Pr oxides.

It can be observed in Fig. 10 that most Pt nanoparticles range from sizes between 1 and 10 nm for all electrocatalysts. However, in some cases much larger particles could be observed as shown in the inset. The largest particles are associated with the Pt/C electrocatalyst, as already deduced from the TEM images in Fig. 9. For the Pt/C sample, the mean particle size increased from 3.4 to 12.8 nm during the long term CA test. In contrast, the mean particle size of Pt

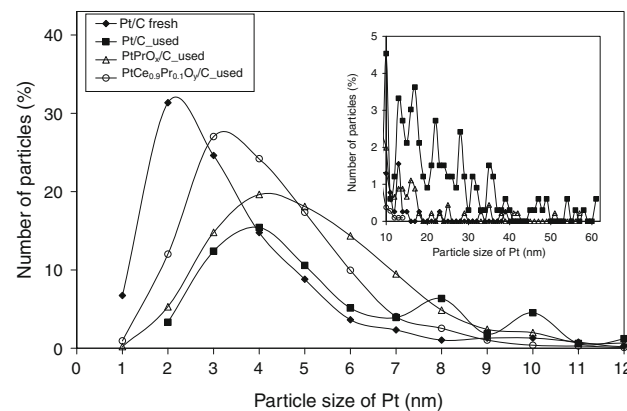


**Fig. 10** TEM-estimated particle size distribution of Pt

remained small in Pr-containing electrocatalysts after the tests (5.9 nm for  $\text{PtPrO}_x/\text{C}$  and 3.7 nm for  $\text{PtCe}_{0.9}\text{Pr}_{0.1}\text{O}_y/\text{C}$ ). The Pt size distributions of the used electrocatalysts suggest that Pt particles grew by particle–particle collisions (coalescence mechanism of sintering [38]), because Pt size distributions are characterized by the absence of Pt particles below a certain size, a maximum value on the small-particle side and a tail towards the large-particle side [39].

#### 4 Conclusions

The study of the effect of praseodymium oxide and cerium–praseodymium mixed oxide in Pt electrocatalyst performance for oxygen reduction reaction in PAFCs allows the following conclusions:

- The  $\text{PtPrO}_x/\text{C}$  and  $\text{PtCe}_{0.9}\text{Pr}_{0.1}\text{O}_y/\text{C}$  electrocatalysts demonstrated a slightly improved catalytic activity towards ORR in comparison to the reference Pt/C electrocatalyst.
- The deviation of the Tafel slope in the low current density region from that in the high current density region is very little on  $\text{PtPrO}_x/\text{C}$  and  $\text{PtCe}_{0.9}\text{Pr}_{0.1}\text{O}_y/\text{C}$ , which indicates that PtOH film formation was greatly inhibited by Pr and Ce–Pr oxides.
- The activity decay of the electrocatalysts during the long term CA tests was slower on  $\text{PtPrO}_x/\text{C}$  and  $\text{PtCe}_{0.9}\text{Pr}_{0.1}\text{O}_y/\text{C}$  than on Pt/C.
- The Pr and Ce–Pr oxides improved Pt dispersion on the fresh electrocatalysts with regard to the Pt-only catalyst.
- In spite of the Pr and Ce–Pr oxides dissolution under the reaction conditions of the long term CA tests, they were able to partially prevent Pt sintering. The high Pt dispersion remained even after the metal oxides leached to the reaction medium.

**Acknowledgments** The authors thank the financial support of the Spanish Ministry of Science and Innovation (project CIT-420000-2009-48, which is co-funded with FEDER resources).

## References

1. Sammes N, Bove R, Stahl K (2004) *Curr Opin Solid State Mater Sci* 8:372
2. Shao Y, Yin G, Gao Y (2007) *J Power Sources* 171:558
3. Jalan VM (1980) US Patent 4 202 934
4. Jalan VM, DA Landsman (1980) US Patent 4 186 110
5. Landsman DA, Luczak FJ (1983) US Patent 4 373 014
6. Landsman DA, Luczak FJ (1982) US Patent 4 316 944
7. Watanabe M, Tsurumi K, Mizukami T et al (1994) *J Electrochem Soc* 141:2659
8. Stonehart P (1992) *J Appl Electrochem* 22:995
9. Fuller TF, Luczak FJ, Wheeler DJ (1995) *J Electrochem Soc* 142:1752
10. Seo A, Lee J, Han K, Kim H (2006) *Electrochim Acta* 52:1603
11. He Q, Mukerjee S, Zeis R et al (2010) *Appl Catal A* 381:54
12. Krishna K, Bueno-López A, Makkee M et al (2007) *Appl Catal B* 75:189
13. Krishna K, Bueno-López A, Makkee M et al (2007) *Appl Catal B* 75:201
14. Krishna K, Bueno-López A, Makkee M et al (2007) *Appl Catal B* 75:210
15. Parres-Eslapez S, Illán-Gómez MJ, Salinas-Martínez de Lecea C et al (2010) *Appl Catal B* 96:370
16. Glass JT, Cahen GL Jr (1988) *J Electrochem Soc* 135:1650
17. He Q, Mukerjee S, Shyam B et al (2009) *J Power Sources* 193:408
18. Higuchi E, Uchida H, Watanabe M (2005) *J Electroanal Chem* 583:69
19. Ardizzone S, Trasatti S (1996) *Adv Colloid Interface Sci* 64:173
20. Weber M, Nart FC, de Moraes IR et al (1996) *J Phys Chem* 100:19933
21. Liu Z, Wainright JS, Savinell RF (2004) *Chem Eng Sci* 59:4833
22. Crabb EM, Marshall M, Thompsett D (2000) *J Electrochem Soc* 147:4440
23. Shih Y, Sagar GV, Lin SD (2008) *J Phys Chem C* 112:123
24. Neyerlin KC, Gu W, Jorne J et al (2006) *J Electrochem Soc* 153:A1955
25. Lima FHB, Gonzalez ER (2008) *Electrochim Acta* 53:2963
26. Giacomini MT, Ticianelli EA, McBreen J et al (2001) *J Electrochem Soc* 148:A323
27. Markovic NM, Schmidt TJ, Stamenkovic V et al (2001) *Fuel Cells* 1:105
28. He Q, Mukerjee S (2010) *Electrochim Acta* 55:1709
29. de Sena DR, Gonzalez ER, Ticianelli EA (1992) *Electrochim Acta* 37:1855
30. Kauffman DR, Tang Y, Kichambare PD et al (2010) *Energy Fuels* 24:1877
31. Ross PN (1980) Oxygen reduction on supported Pt alloys and intermetallic compounds in phosphoric acid. EPRI-EM-1553. EPRI, Palo Alto
32. Toda T, Igarashi H, Uchida H, Watanabe M (1999) *J Electrochem Soc* 146:3750
33. Bindra P, Clouser SJ, Yeager E (1979) *J Electrochem Soc* 126:1631
34. Lo Nigro R, Toro RG, Malandrino G et al (2003) *Adv Mater* 15:1071
35. Ma L, Chen WX, Zhao J, Zheng YF (2007) *J Crystal Growth* 303:590
36. Hussein GAM, Balboul BAA, Warith MAA et al (2001) *Thermochim Acta* 369:22
37. Atribak I, Bueno-López A, García-García A (2008) *J Catal* 259:123
38. Ascarelli P, Continia V, Giorgi R (2002) *J Appl Phys* 91:4556
39. Granqvist CG, Buhrman RA (1976) *J Catal* 42:477